

Measurements of an Oceanic Front Using a Front-Following Algorithm for AVHRR SST Imagery

A. G. P. Shaw* and R. Vennell*

The Subtropical Front (STF) is a global front which extends around the Southern Ocean and is the boundary where the Subantarctic Surface Water mass (SAW) converges with the Subtropical Surface Water mass (STW). The Southland Front (SF) is part of the STF, which lies off the east coast of the South Island, New Zealand. The SF is narrow, approximately 8 km, with a temperature difference of approximately 1.8°C which can be detected using remote sensing Advanced Very High Resolution Radiometer (AVHRR) sea surface temperature (SST) data. The work presented here is an application of remote sensing for the first detailed study of the surface spatial and temporal variability of the SF. The variability of the SF was quantified using an algorithm developed to follow the Front using AVHRR SST imagery. The algorithm used a new approach to determine the position, mean SST, SST difference, width, and gradient across the Front. Three time scales of variability were examined: long-term (3 years), annual, and seasonal. The algorithm efficiently followed the SF and consistently showed the 3-year mean position was stable and constrained by the bathymetry of the continental slope. Seasonally, the front moved inshore during summer. The temperature gradient across the front was strongest and the front narrowest in winter. The decrease in SST gradient during the 3-year data set coincided with the decrease in Southern Oscillation Index (SOI). ©Elsevier Science Inc., 2001

INTRODUCTION

Remote sensing can be applied to oceanography to show oceanic structures such as fronts. Oceanic fronts occur where two water masses meet and are important physically, biologically, and chemically. The interaction between the water masses can create upwellings, downwellings, plumes, eddies, and meandering. The Subtropical Front (STF) or Subtropical Convergence Zone in the Southern Ocean is a large scale ocean front and is a major region of biological productivity and possibly a major Southern Hemisphere CO₂ sink. It is the boundary where the cool, low-salinity, nutrient-rich Subantarctic Surface Water mass (SAW) converges with the warm, high-salinity, nutrient-poor Subtropical Surface Water mass (STW). The cool dense SAW sinks at the STF, which is found around the globe at an approximate latitude of 40°S (Deacon, 1937; 1945). South of Australia the STF has no sharp front and appears to be further south than in other oceans, located at approximately 42–44°S (Fig. 1a; Deacon, 1937). Lutjeharms et al. (1993) also found that the STF appeared to be diffuse in the South Atlantic Ocean, particularly on the western side of the midocean ridge, describing the surface expression of the STF as intermittent rather than weak. Belkin and Gordon (1996) classify the STF as two fronts around the globe, which they name the South and North STF and which merge together as the Front approaches Western Australia from the west and continues as one front as it passes New Zealand. They referred to the STF in previous articles as relating to either the combination of the two fronts or the South STF.

New Zealand spans the latitudes where the STF is typically found, and as the STF approaches New Zealand, it is deflected south by the land mass (Garner, 1954). The Southland Front (SF) examined here is part of the global STF that lies close to the southern east

* Department of Marine Science, University of Otago, Dunedin, New Zealand

Address correspondence to A. G. P. Shaw, James Rennell Div., Southampton Oceanography Ctr., European Way, Southampton, SO14 3ZH, UK. E-mail: Andrew.G.P.Shaw@soc.soton.ac.uk

Received 4 November 1999; revised 26 June 2000.

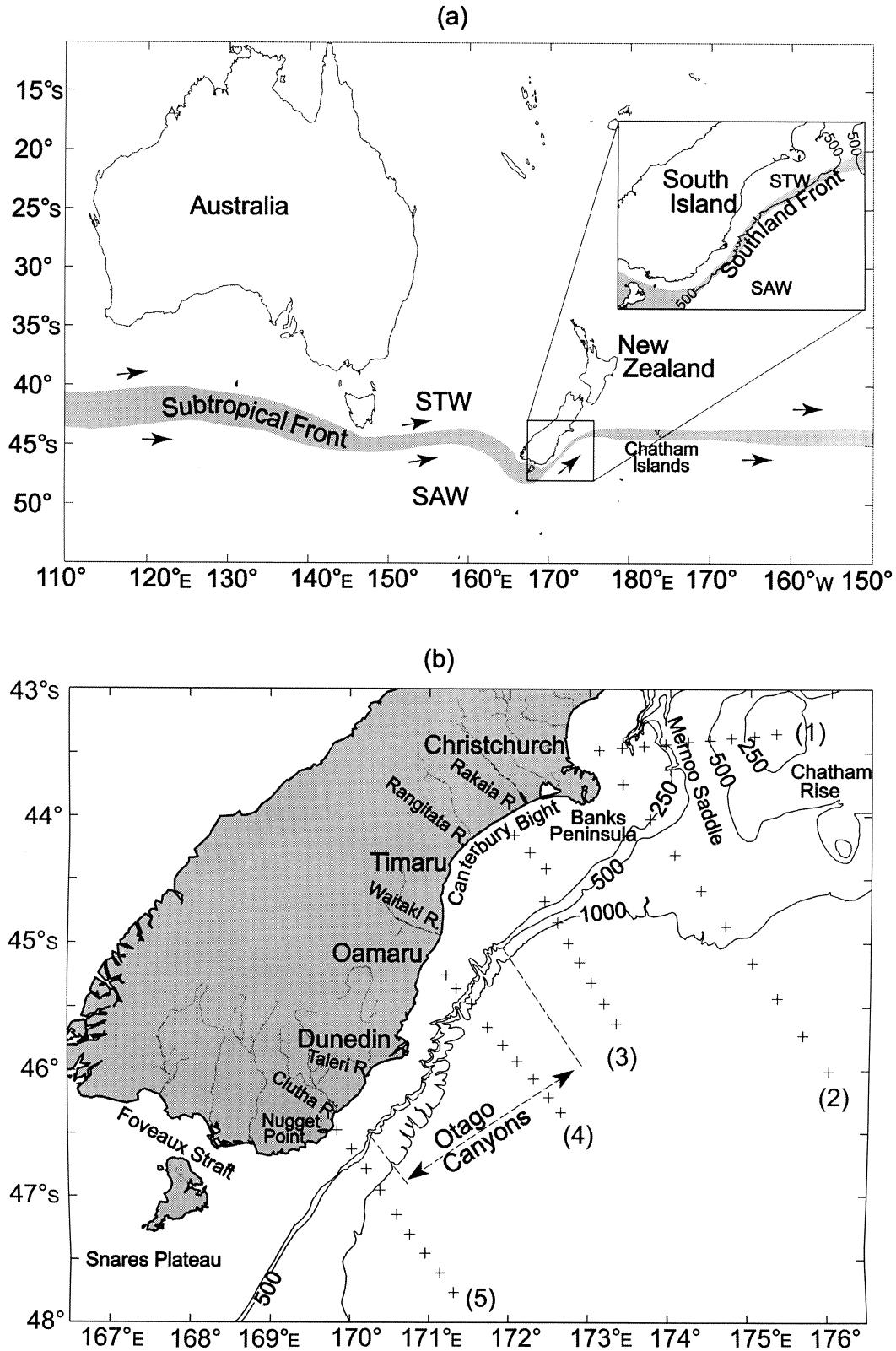


Figure 1. The approximate position of the Subtropical Front (STF) in the southwest Pacific Ocean where the Subantarctic Surface Water mass (SAW) and the Subtropical Surface Water mass (STW) converge; and the location of the Southland Front off the South Island, New Zealand: (a) conductivity temperature depth (CTD) stations (+) from five transects (1–5) of the NIWA (NZOI) cruise 3006 in April 1993, from the ship *RV Akademik Lavrentyev* (b).

coast of the South Island, New Zealand, and can be clearly seen in Advanced Very High Resolution Radiometer (AVHRR) sea-surface temperature (SST) imagery. Garner (1959) showed that in New Zealand surface waters, the STF followed approximately the isotherms of 15°C in February (summer) and 10°C in August (winter), but its isohalines varied little between these seasons. Heath (1975) described the SF as a gradual change in the hydrological properties rather than an abrupt change.

The SF is bounded by the Southland Current (SC) on its western side, containing mostly STW, and SAW to the east. The SC extends from the coast to the SF and has a high salinity subsurface core (Jillett, 1969; Heath, 1972; Chiswell, 1996). The geostrophic velocity of the SC relative to 500 dbar has been calculated at 20 cm s⁻¹ (Heath, 1975). In 1993, Chiswell (1996) examined the variability of the SC by deploying current meters at five locations within the SC, at Oamaru, Nugget Point, Foveaux Strait, east and west Snares Plateau (Fig. 1b). He showed that the mean velocity of the SC over the shelf off Nugget Point and Oamaru had recorded mean flow rates of 24 cm s⁻¹ and 14 cm s⁻¹, respectively. These current meter observations were compared with wind velocity data, and Chiswell concluded that the temporal variabilities in velocity of the SC over the shelf were principally driven by winds over the Snares Plateau and in Foveaux Strait within the weather band time scale of approximately 1–14 days. Chiswell (1996) also calculated total volume transport through the transects off Oamaru and Nugget Point (transect 4 and 5, Fig. 1b) as 10.4 Sv and 2.2 Sv, respectively (1 Sv=10⁶ m³ s⁻¹), using conductivity temperature depth (CTD) data. Jillett (1969) found that in spring and summer, the SAW moved over the STW, near to the surface. Thus, the SF at the surface is closer inshore during these months.

Off the Canterbury coast at latitude 43°30'S, an underwater ridge known as the Chatham Rise acts as a partial barrier to the flow of SAW and STW. The Mernoo Saddle is located near the western end of the Chatham Rise, approximately 100 km east of Banks Peninsula (Fig. 1b). The Saddle has an approximate width of 40 km and a maximum depth of 580 m. Burling (1961) observed a low salinity and low temperature tongue extending through the Mernoo Saddle from the south. Heath (1972) referred to this northward flow through the Saddle as an extension of the SC as it had similar hydrological properties to the subantarctic component of the SC. However, Shaw and Vennell (2000a) described it as a “plumelike” wisp of subantarctic waters (SAW wisp) extending north through the Saddle. The STF continues east along the Chatham Rise to the Chatham Islands and beyond. Currents over the Chatham Rise are dominated by diurnal tides (along-rise) and semidiurnal tides cross-rise (Chiswell, 1994a), and the net flow along the Chatham Rise is eastwards. Barnes (1985), using satellite SST imagery, showed velocities of 5 cm s⁻¹ or less. Heath

(1983, Table 1) measured 4.6 cm s⁻¹ at a current meter at a depth of 43 m on the Rise, and Chiswell (1994a) estimated the geostrophic velocity (relative to 500 dbar) to be 6.0 cm s⁻¹.

Little is known about the variability of the STF, and there are very few quantitative measurements of the characteristics of large scale ocean fronts. The aim of this study is to use a new remote sensing technique to determine the spatial and temporal variability in the position and characteristics (SST gradient, width and cross-front temperature difference) of the Southland Front (SF), part of the large scale STF. The variability in the position of the SF should reflect the stability and dynamics of the Front, for example the extent of topographic steering in this region. Determining the SST gradient of the SF can provide some indication of the spatial and temporal variability of the relative velocity flow of the SF. In addition, the SF has commercial and biological implications as it forms a major barrier for many marine species. For example, the SF divides the distribution of two squid species, the commercially important *Nototodarus sloanii* and *Moroteuthis ingens*, important in the marine ecosystem as a prey species for mammals, birds, and some fish (Jackson et al., 2000). AVHRR SST data were analyzed over three time scales, a 3-year period (1989–1992), annually, and seasonally.

METHOD

The SF was examined using a 3-year archive (April 1989–March 1992) of twice daily AVHRR SST images, with a pixel resolution of 1' of arc (approximately 1.3 km easting×1.8 km northing at midlatitudes). The processing and preparation of the images and the cloud detection techniques used are described in Shaw et al. (1999) and in Shaw and Vennell (2000a,b). The SST algorithm was based on Barton (1982), which applies the “split window” technique using Bands 4 and 5 (11 μm and 12 μm bands, respectively) that corrects for atmospheric water vapor. A total of 277 AVHRR SST images were moderately free of cloud in the study area. This area covered the region from latitude 44°S to 48°S and eastwards from longitude 169°E to 174°E, spanning the SF off the east coast of New Zealand.

The standard remote sensing techniques such as gradient operators, edge detectors, and line enhancers do not describe ocean fronts using physical parameters such as mean temperature, width, and temperature difference across the front, nor monitor the variability of these parameters along the front. Thus, to determine the spatial and temporal variability of the SF, a Front-Following Algorithm was developed to follow the SF in AVHRR SST imagery, determining both the position and specific characteristics of the Front (described in Shaw and Vennell, 2000b). These characteristics were mean SST (T_0), width ($2a$), SST difference ($2b$) and gradient ($-b/a$) across the

Front. A hyperbolic tangent function was fitted to SST data extracted from within a window using least-squares to estimate the position and characteristics of the Front. Assuming that only one front is represented, then the hyperbolic tangent function describing a surface of the idealised oceanic front (Fig. 2) was assumed to be (Shaw and Vennell, 2000b) [Eq. (1)]

$$Temp = T0 + b \tanh \left[\frac{-X' \cos(\theta) - Y' \sin(\theta) + C}{a} \right]. \quad (1)$$

The parameters are defined with respect to the line of inflection (LI) of the hyperbolic tangent surface:

$T0$ = mean temperature of the two water masses, i.e., the temperature at LI (°C),

a = across-front scale (km), where a represents the horizontal distance over which the temperature change is 76.2% of b , and $2a$ is assumed to be the width across the front,

b = half the temperature difference across the thermal front (°C),

θ = direction (angle) between the Y' axis and the line of inflection, i.e., the frontal direction relative to the extraction window,

C = perpendicular distance from the center of the extraction window to the LI of the front (km),

X' and Y' = coordinates in the system relative to the extraction window (km).

To initiate the algorithm, a point was manually selected close to the SF. The first window was orientated to the quadrant nearest to the front's direction, and the function was fitted to the data using least-squares to estimate the initial orientation of the window (ψ), that is, $\psi = \theta$. The window was then rotated normal to the front and the function refitted to the data. The Algorithm then stepped along the front by moving the rotated extraction window 2 km in the direction of the front estimated from the current window, using translation parameter C and θ . With each step, the orientation of the extraction window was updated, that is, $\psi_{\text{new}} = \psi_{\text{old}} - \theta_{\text{old}}$. The size of the extraction window was 30 km \times 20 km (i.e., a width of 30 km across-front and 20 km along-front). However, fine features such as plumes are narrow and the extraction window extended beyond the width of the plume. For these features a smaller extraction window was used having a width of 20 km.

Nonlinear least-squares solutions which failed to converge (<1% difference between successive iterations of parameter estimations and convergence to be reached within 50 iterations) or whose estimated parameters lay outside set parameter bounds (Shaw and Vennell, 2000b, Table 1) were rejected. The rejected solutions were not included in these analyses. Figure 3 shows an example of the algorithm tracking a plume protruding from the

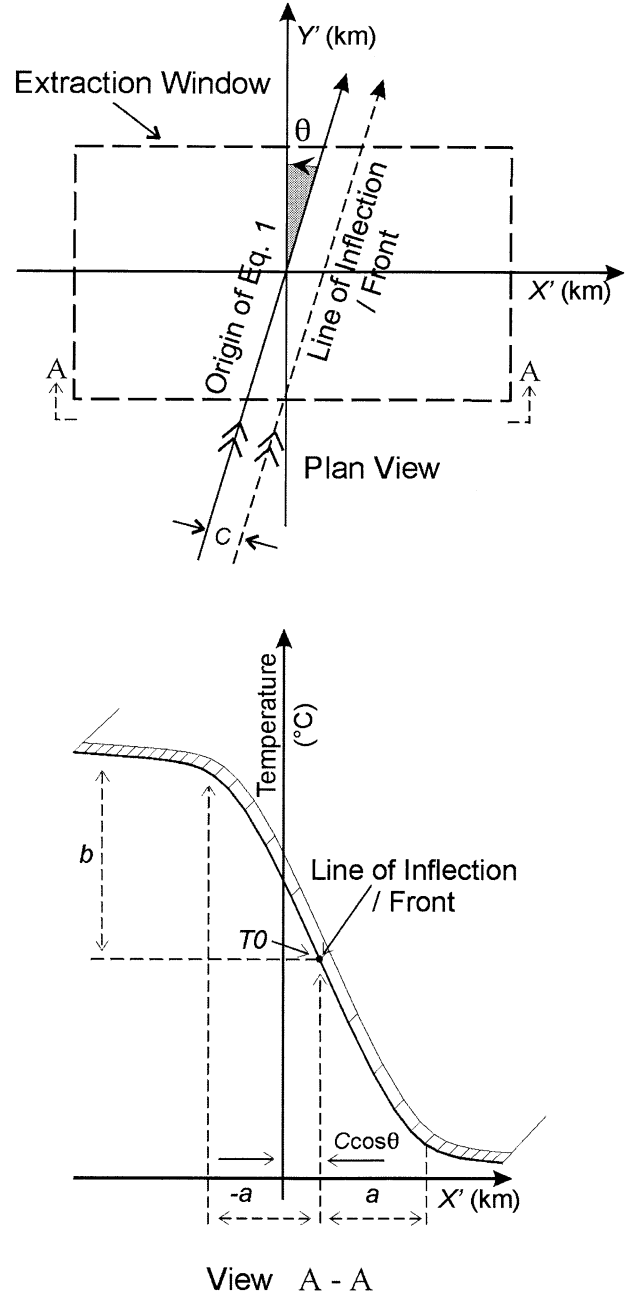


Figure 2. A plan view and side view of the surface representation of a thermal oceanic front illustrating the parameters of the hyperbolic tangent function [Eq. (1)]. Reproduced from Shaw and Vennell (2000b).

SF. The dotted line in Figure 3 indicates that the algorithm did not reach a solution; however, there was still enough information to track the plume. In some images, only segments of the SF could be seen due to cloud contamination. There were occasions where the algorithm had difficulties tracking the front due to a sudden change in direction exceeding approximately 90° (Shaw and Vennell, 2000b), for example, around some plumes. When this occurred, the algorithm was terminated and then restarted beyond the termination point. Thus, each image

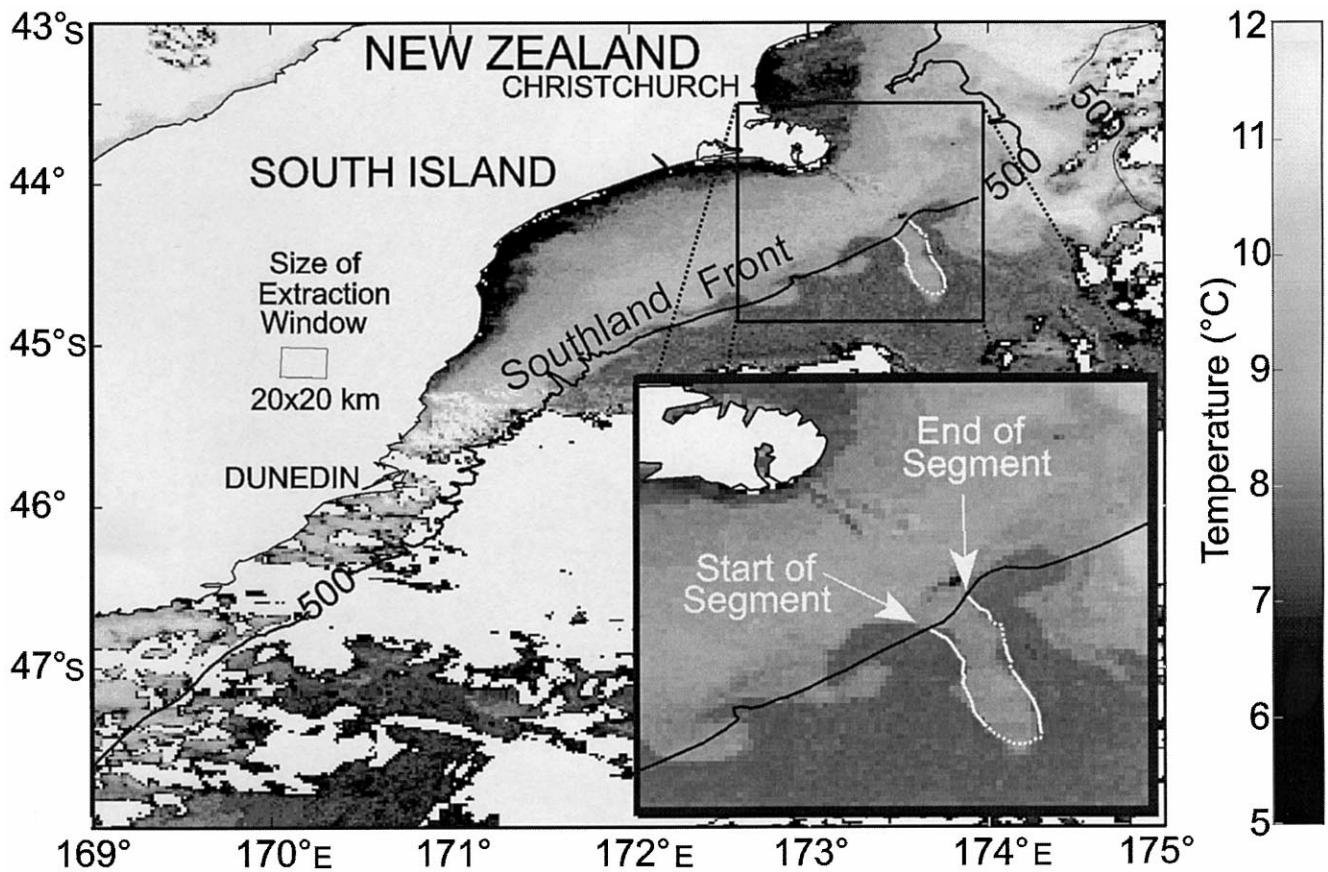


Figure 3. An AVHRR SST image (25 July 1989 at 15.03 h NZST) showing an oceanic plume (enlarged in inset) protruding from the Southland Front tracked using the algorithm. The dotted lines represent the regions where the parameter requirements of the algorithm were not met.

may contain more than one segment where the algorithm could follow the Front. Multiple fronts close to the New Zealand coast were assumed to be Neritic fronts. Segments of the SF were distinguished using the following criteria. First, the temperature difference ($2b$) of the SF was approximately $2 \pm 0.5^\circ\text{C}$ and, second, the mean temperature (T_0) was similar ($\pm 0.3^\circ\text{C}$) from one segment to the next.

The data from the algorithm estimating the position of the SF were “binned” in time (three time scales) and space. The first time scale was the 3-year data set (April 1989–March 1992), the second was three separate years (each from April to the following March), and the third a seasonal time scale. The seasons were defined as autumn (March–May), winter (June–August), spring (September–November), and summer (December–February). The mean position of the SF over each time scale was determined using spatial binning of the frontal position. The data were divided into 20 km bins, with no overlap, such that the bins were independent from one another. Given that Heath (1981a) suggested that the SF may be influenced by the bathymetry of the continental slope, and that the continental slope off the east coast of the South

Island lies in the northeast direction, then the bins were orientated across the northeast bearing. The dimensions of the bins were 20 km long in the northeast direction approximately parallel to the SF and 220 km wide (perpendicular to the northeast path) to ensure all information on the SF was contained. The distance covered was 450 km from a starting point at 2235 E km 5310 N km NZMG (latitude $47^\circ 21' 51''\text{S}$, longitude $169^\circ 21' 55''\text{E}$) and ended near Banks Peninsula at 2553.2 E km 5628.2 N km (latitude $44^\circ 38' 37''\text{S}$, longitude $173^\circ 32' 39''\text{E}$). The results from the binned data were calculated in New Zealand Map Grid (NZMG, Lands and Survey, 1973) and converted to geographic coordinates when needed. The variability of the Front was calculated perpendicular to the northeast path within each bin and indicated by standard deviation (*s.d.*) bars.

The position of the SF estimated from the algorithm was compared with CTD data to ground truth the results of the algorithm. The CTD measurements were made during the National Institute of Water and Atmosphere (NIWA), New Zealand Oceanographic Institute (NZOI) cruise 3006, from the ship *RV Akademik Lavrentyev*, in April 1993 (Chiswell, 1996). This cruise covered five

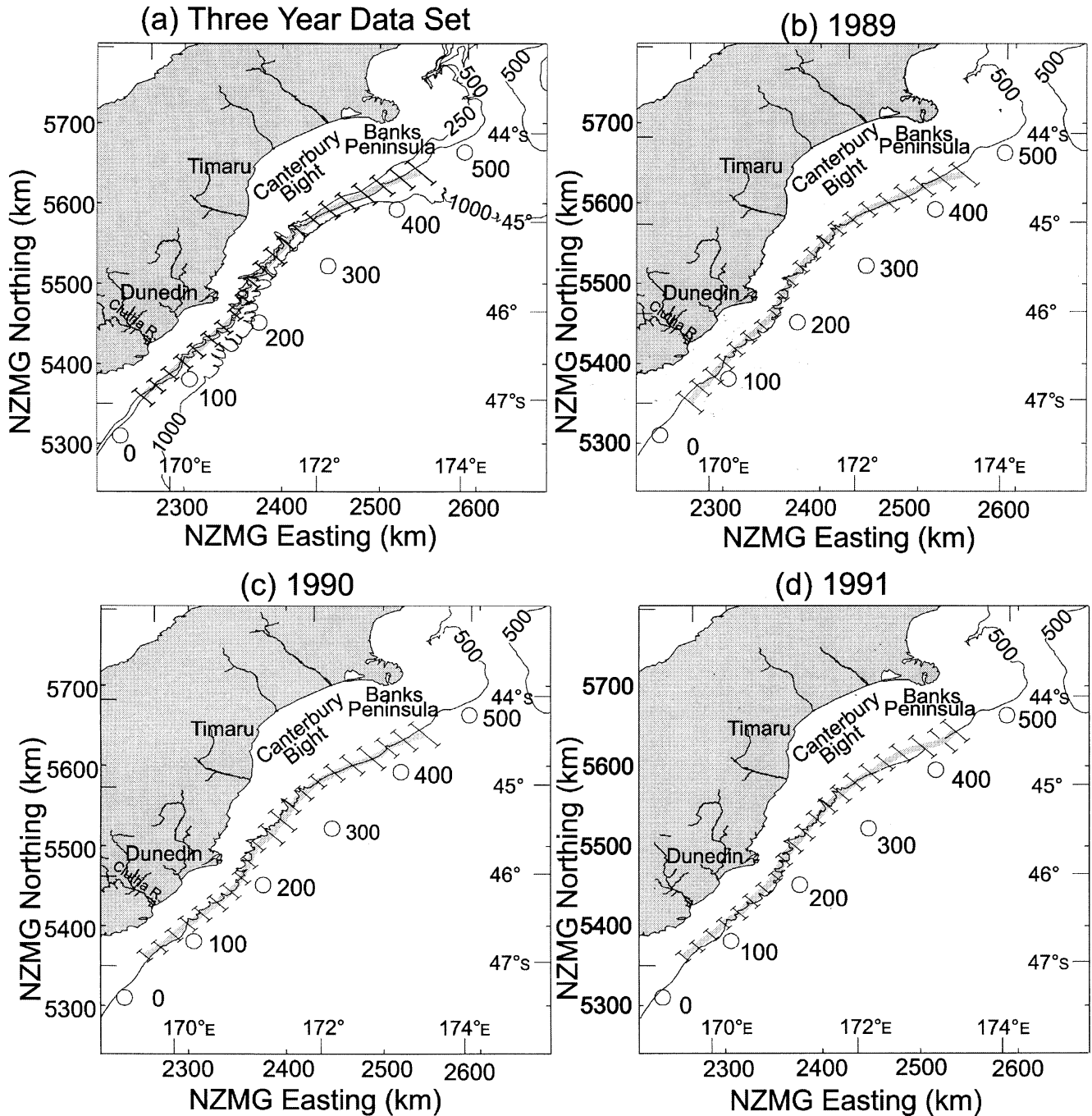


Figure 4. Average position (± 1 s.d.) of the Southland Front for: a) the 3-year period (April 1989–March 1992); b) 1989 (April–March); c) 1990 (April–March); d) 1991 (April–March). Each year was defined from April to March of the following year. The rms of the S.D.s in the position of the SF for each time scale is shown in Table 2. The circles show the distance (km) along the northeast path for the binning process.

transects within or near this study area off the east coast of the South Island, New Zealand.

RESULTS

Position of the Southland Front

The mean position of the SF from the 3-year data set is shown in Figure 4a and the mean for the three separate

years are presented in Figures 4b–d. Figure 4a shows that the mean position of the SF appears to be influenced by the bathymetry of the continental slope. The first 50 km of the southern end of the Front contained very few images and was removed before the analysis of the results as the data may not give an appropriate spatial representation of the SF.

The mean offset in the position of the SF relative to

Table 1. The Overall Mean Offset in the Position of the Southland Front (SF) Relative to the 500 m Isobath, Calculated Perpendicular to the Northeast Path for Each Time Scale^a

Time Scales	Offset (km)±S
3-year period	0.55±0.11
1989 (Apr–Mar)	0.31±0.19
1990 (Apr–Mar)	1.92±0.18
1991 (Apr–Mar)	−1.68±0.21
Autumn (3-year average)	−2.84±0.18
Winter (3-year average)	4.66±0.19
Spring (3-year average)	4.28±0.25
Summer (3-year average)	−8.48±0.19

^a A negative sign indicates that the SF is further inshore; S is the unbiased estimator of the standard error of the mean.

the 500 m isobath, calculated perpendicular to the northeast line for the 3-year period was 0.55 km with an unbiased estimator of the standard error of the mean (S.E.M.) “S” (von Storch and Zwiers, 1999) of 0.11 km (Table 1). The minimum variation in the position of the SF ($s.d.$ = 8 km) occurred off Dunedin (Table 2, Fig. 4a). The maximum standard deviation of position (19 km) occurred in the Canterbury Bight. The root mean squared (rms) of the $s.d.$ ’s was 12.0 km (Table 2). The steepest gradient of the continental slope can be seen offshore and just north of Dunedin, after which the gradient decreases toward the Chatham Rise (Fig. 1b). Figures 4a–d show that there is a good visual correlation between the decreasing gradient of the continental slope and the increasing variability in the position of the SF about the mean.

When the three years (April–March) were examined separately (Figs. 4b–d, Table 1), the mean position of the SF was also found to be located near the mid-point of the continental slope. Thus annually, the overall mean position of the Front relative to the 500 m isobath was very consistent, approximately within 1 pixel (1.3 km easting×1.8 km northing, Table 1), indicating that the position may be strongly influenced by the continental slope. However, the seasonal analysis revealed that the position of the Front during the summer months was the furthest inshore compared with the other seasons (Table 1). One-way ANOVA’s showed significant differences (at the 99% confidence interval) in position relative to the 500 m isobath between seasons ($F=645$, d.f.=3 & 21,959) and years ($F=78.33$, d.f.=2 & 21,960). Figure 5 illustrates the mean position of the SF during summer being inshore from the 500 m isobath and the mean position from the 3-year data set. The mean position during winter is shown near or slightly offshore from the 500 m isobath.

The rms of the $s.d.$ ’s for each time scale from the 220 km×20 km bins along the SF are presented in Table 2, with minimum and maximum values. Annually, there was more variability in the mean position of the front during 1990 than 1989 or 1991 (Table 2a). Seasonally,

the position of the front was more variable during spring than the other seasons (Tables 2b–c). The greater variability in the position of the SF was influenced by the presence of plumes and meanders in the SF. Plumes were found to be in greater numbers north of the Otago Canyons (Fig. 1b), and a relative increase in the number of plumes was observed in the spring and summer during the El Niño year of 1991 (Shaw, 1998). This was consistent with higher values of maximum variability ($s.d.$) for this time compared with 1989 and 1990 (Table 2b). In addition to plumes, there appeared to be more meandering of the SF during spring but this was not quantified in this study. More data and further work are needed to determine the mechanism of this meandering. There was a potential bias in the data for autumn 1989 as the month of March was missing. To determine the extent of this bias, the rms of the $s.d.$ values were recalculated for autumn 1990 and 1991 with the March data removed, and the recalculated values were compared with the original autumn rms values. This analysis revealed that rms of the $s.d.$ were under estimated by up to 18% with the March data missing.

Characteristics of the Southland Front

The characteristics (parameters) of the SF, that is, the width $2a$, temperature difference $2b$, mean temperature T_0 , and the temperature gradient $-b/a$ are shown spatially along the SF for the 3-year time scale (Fig. 6). The mean value of the individual observations over the length of the SF for each parameter is shown in Table 3 for all temporal comparisons. The potential bias due to missing data for autumn 1989 was examined using the same technique described in the previous section. The analysis showed that the parameter estimates in Table 3b for autumn 1989 were underestimated by up to 11%.

The mean width ($2a$) of the SF over the three years was 8.36 km, the mean temperature difference ($2b$) between the two water masses (STW and SAW) was 1.76°C, the mean gradient ($-b/a$) was $-0.28^\circ\text{C}/\text{km}$ and the mean temperature (T_0) of the SF was 11.01°C (Table 3a). The width ($2a$) tended to decrease slowly as the STW and SAW moved northeast along the coast (Fig. 6a). This trend in $2a$ was also seen in the separate years and in three seasons (autumn, winter, and summer), although, in spring, the width remained reasonably constant (Shaw, 1998). Figure 6b shows the temperature difference ($2b$) was highest in the 100 km stretch of the SF between the Clutha River outlet (at 100 km along the northeast line; Fig. 4a) and just beyond Dunedin (at 200 km). This was consistent throughout all the time scales. The average temperature difference of this region of the SF from the 3-year AVHRR SST data set was 2°C . The temperature difference steadily decreased from this level to 1.5°C near Banks Peninsula. The temperature gradient ($-b/a$) was reasonably constant at $-0.28^\circ\text{C}/\text{km}$, although there was some variation south of the Clutha River outlet, be-

Table 2. Variability about the Mean Position of the Southland Front^a

<i>a. The 3-Year and Annual Time Scales, April 1989–March 1992</i>					
		1989 (Apr–Mar)	1990 (Apr–Mar)	1991 (Apr–Mar)	3-Year Total
Max no. images		94	109	74	277
rms <i>s.d.</i> (km)		11.1	12.6	11.5	12.0
Max <i>s.d.</i> (km)		18.2	19.5	18.2	19.0
Min <i>s.d.</i> (km)		6.3	7.3	6.4	8.0
<i>b. The Seasonal Time Scales of 1989, 1990, and 1991</i>					
		Autumn ^b (Mar–May)	Winter (Jun–Aug)	Spring (Sep–Nov)	Summer (Dec–Feb)
1989	Max no. images	12	24	23	23
	rms <i>s.d.</i> (km)	9.0	7.7	11.3	9.1
	Max <i>s.d.</i> (km)	19.4	14.4	19.0	18.3
	Min <i>s.d.</i> (km)	1.9	4.0	6.4	2.9
1990	Max no. images	33	24	32	24
	rms <i>s.d.</i> (km)	8.9	12.4	13.2	9.1
	Max <i>s.d.</i> (km)	15.5	22.9	22.6	15.6
	Min <i>s.d.</i> (km)	2.1	6.7	7.3	4.1
1991	Max no. images	24	19	16	18
	rms <i>s.d.</i> (km)	10.2	10.9	13.8	9.6
	Max <i>s.d.</i> (km)	17.3	17.8	26.7	19.1
	Min <i>s.d.</i> (km)	2.9	2.5	4.0	2.2
<i>c. The Averaged Seasons for the 3 Years, April 1989–March 1992</i>					
Averaged Seasons		Autumn (Mar–May)	Winter (Jun–Aug)	Spring (Sep–Nov)	Summer (Dec–Feb)
Max no. images		74	67	71	65
rms <i>s.d.</i> (km)		9.7	11.4	12.9	9.1
Max <i>s.d.</i> (km)		15.7	17.5	21.0	17.7
Min <i>s.d.</i> (km)		5.9	6.9	7.4	5.1

^a Maximum and minimum standard deviations (*s.d.*) in the local position of the Southland Front and rms values of the *s.d.* along the front.

^b No data for March 1989.

tween 50 km and 100 km along the northeast line (Fig. 6c). The negative sign of the temperature gradient refers to a decrease in temperature across the SF from the STW to SAW. The mean temperature T_0 of the 3-year time scale increased approximately 1.5°C as the STW and SAW moved northeast along the SF.

Table 3a shows the inter-annual variations with the parameters averaged in years. The width across the front ($2a$) had a range of 1.40 km over the 3 years, and increased steadily from 1989 to 1991. Applying a one-way ANOVA to the 3-year data set revealed that there was a significant difference in width between years at the 99% confidence interval ($F=137.6$, d.f.=2 & 21,960). This increase over the years is also seen in Table 3b. This range of 1.40 km is similar to one pixel in the AVHRR SST image, indicating a small but significant variation in width. Both the mean temperature difference ($2b$) and temperature gradient ($-b/a$) across the front between the STW and SAW decreased from 1989 to 1991 (Table 3a). The interannual differences were significant at the 99% confidence interval for both parameters ($F=887.9$, d.f.=2 & 21,960 for $2b$; $F=305.7$, d.f.=2 & 21,960 for $-b/a$). This trend is also generally seen in Table 3b, where 1991 has the lowest temperature difference and temperature gradient for each season. The mean temper-

ature (T_0) at the interface of the SF cooled significantly between 1989 and 1991 ($F=555.8$, d.f.=2 & 21,960, significant at the 99% confidence interval).

The seasonal comparisons of the estimated parameters of the SF are shown in Table 3b–c. Although the parameters $2a$ and $2b$ of the SF had small variations between seasons, there were still trends in the data. The width ($2a$) across the SF was generally lowest in winter and highest in summer. The spring season showed the greatest range in width over the 3 years (range=2.77 km) and the summer had the lowest range (0.6 km). The temperature gradient was consistently higher in winter than the other seasons during the three years. The mean temperature (T_0) at the interface of the SF showed seasonality, that is, coolest during winter and warmest in summer. The temperature difference had no consistent seasonality. The greatest variability between the seasons occurred in 1989, which had a greater range of parameter estimates compared with 1990 and 1991 (Table 3b).

DISCUSSION

Position of the Southland Front

This study shows that the SF was closely coupled to the bathymetry. The observations summarized in Figure 4

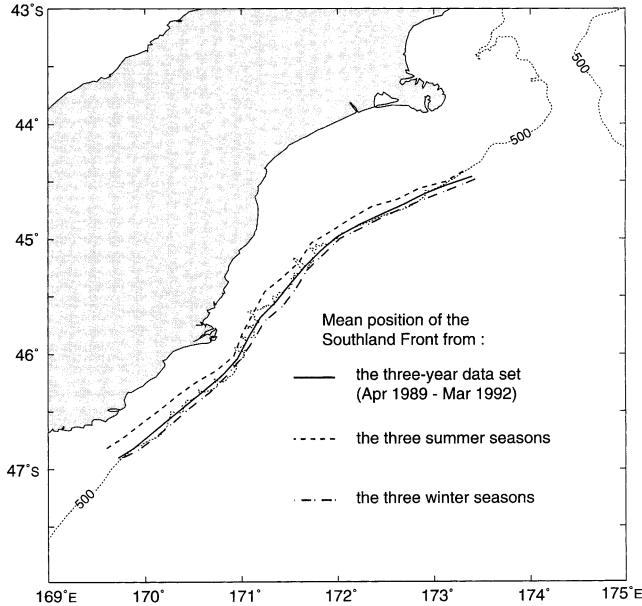


Figure 5. The mean position of the Southland Front from the averaged summer seasons, the averaged winter seasons and the overall 3-year period. The dotted line shows the 500 m isobath.

show that the mean position of the SF followed the 500 m isobath. As the STF approaches New Zealand, it passes through the Snares Depression (south of New Zealand), which has a depth of approximately 500 m (Bradford-Grieve et al., 1991). This supports the suggestion that the depth scale of the STF off the east coast of New Zealand (i.e., the SF) may have an approximate mean depth of 500 m. Below the STF lies the Antarctic Intermediate Water (AIW) approximately 500 m thick (Pickard, 1975) at a depth of 700–1200 m (Table 4). However, the relatively shallow topography just south of New Zealand may cause the lower 200–300 m of the STF to separate from the upper layer and instead flow with the deeper water masses around the Campbell Plateau (southeast of New Zealand) meeting up again east of New Zealand.

A possible mechanism for the STF to follow a (nearly) constant (i.e., 500 m) isobath requires consideration of the conservation of potential vorticity (Pond and Pickard, 1983), which applies to a frictionless and adiabatic environment. Neglecting density variations along the flow, and considering the water column as a whole, this can be written as Eq. (2):

$$\left(\frac{\zeta+f}{D}\right)=\text{const}, \quad (2)$$

where D is the depth of the water column, f is the planetary vorticity (Coriolis parameter), and ζ is the relative vorticity.

Two CTD transects (Fig. 1b, transects 2 and 3) were used to estimate ζ . The $\partial v/\partial x$ component of ζ , where v is the across front velocity and x is the along front dis-

tance, could not be estimated here as there were no data on the cross-front velocity. It was assumed that the shear from the cross-front velocity ($\partial v/\partial x$) was much smaller than the shear from the along-front velocity ($\partial u/\partial y$), that is, $\zeta \approx (\partial u/\partial y)$. The relative vorticity was calculated from CTD geostrophic velocities (Shaw, 1998) determined using the method outlined in Reid and Mantyla (1976) for extrapolating over the shelf. Typical magnitudes for ζ were calculated as $9 \times 10^{-6} \text{ s}^{-1}$ for transect 2, and $1.5 \times 10^{-6} \text{ s}^{-1}$ for transect 3. These ζ values are at least an order of magnitude smaller than the planetary vorticity ($\approx -10^{-4} \text{ s}^{-1}$ at latitude 45°S). Therefore, ζ can be ignored, and the conservation of potential vorticity can be approximated by

$$\left(\frac{f}{D}\right)=\text{const}. \quad (3)$$

Equation (3) represents *topographic steering*, by which the depth of the current (D) can be predicted as it passes around bottom topography. Analytical models have shown that the flow from a large-scale oceanic current deflects around topographic features (Marshall, 1995a) and topographic steering occurs in the Antarctic Circumpolar Current (Marshall, 1995b). Rintoul et al. (1997) suggest the location of the STF between the Tasmanian Continental Slope and the South Tasman Rise may be influenced by topographic steering.

Topographic steering may contribute to the mean position of the SF closely following the 500 m isobath. Figure 7a shows the mean position of the SF from the 3-year AVHRR SST data set with respect to depth, from which potential vorticity was estimated along the Front (Fig. 7b). The dotted and dashed lines represent the depth and potential vorticity at one *s.d.* from the mean position (offshore and inshore, respectively). The *s.d.* in position increases at approximately 250 km (south of Timaru). Plumes (filaments) protruding from the SF have been recorded in this region and in the Canterbury Bight (Shaw, 1998) and are probably the main factor contributing to this increase in variability of the mean position of the SF off the Canterbury Bight. The cause of plume formation is unclear and is outside the scope of this study, but may be due to the undulating bathymetry of the Otago Canyons creating instabilities along the front allowing plumes to propagate and grow as they flow northeast along the SF. Plumes would clearly have both larger positive and negative values of ζ than the mainflow of the SF, and may therefore introduce a bias in the potential vorticity calculation in Figure 7b. Figure 7a indicates that the depth of the SF steadily increases between 50 km and 250 km, probably associated with inertial current effects resulting from the turning of the Continental Slope bathymetry in the region of the Otago Canyons (Fig. 1b). Similar inertial current effects have been conjectured to be important in the separation of the Gulf Stream (Özgökmen et al., 1997).

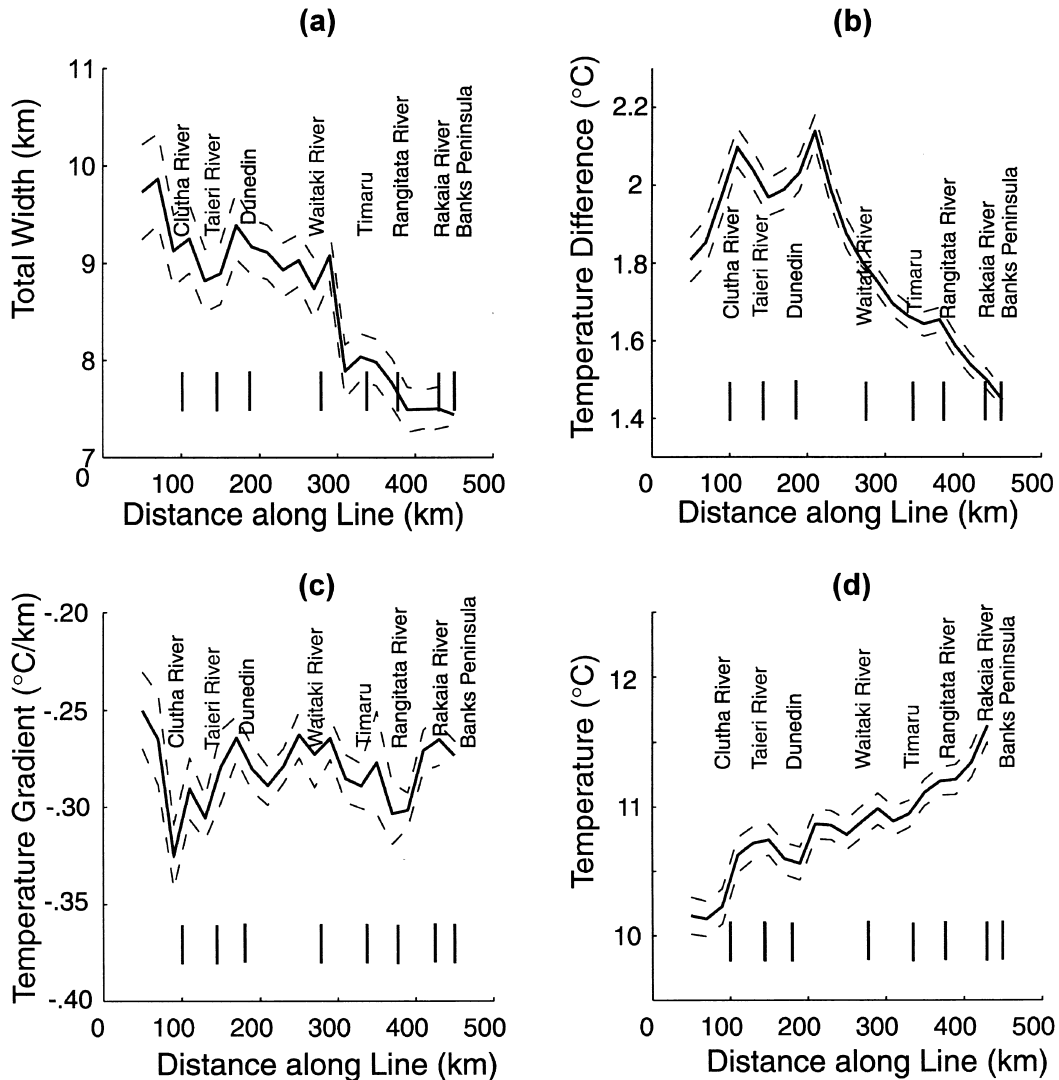


Figure 6. The characteristics (mean \pm S) of the Southland Front, April 1989–March 1992 (3 year AVHRR SST data set), corresponding to the mean position in Figure 4a: a) the total width, 2a; b) temperature difference, 2b; c) temperature gradient, $-b/a$; d) temperature along the front T_0 . S is the unbiased estimator of the S.E.M. (shown dashed). The total number of images is 277.

Within the Canterbury Bight the isobaths diverge (Fig. 1b), and thus Eq. (3) suggests that the fluid flow of the SF should also diverge. It was expected that the width of the SST Front from the 3-year AVHRR data set would increase and the velocity of the flow decrease as the SF moved northwards, but Figure 6a showed a decrease in width along the Canterbury Bight. The reason for this decrease is not clear. However, the divergence of the flow is supported by the volume transport and geostrophic velocities calculated from the CTD transects 2–4. The estimated volume transport through transect 4 was calculated at 10.4 Sv (Chiswell, 1996) and the values through transects 3 and 2 were 8.4 Sv and 8.6 Sv, respectively. The geostrophic velocities calculated from transects 3 and 2 (Shaw, 1998, Appendix A.3) showed a decrease in velocity of the northeast flow from transect 3

to transect 2 and because these transects have a similar estimated volume transport, this suggests that the fluid flow of the SF should diverge. Chiswell (1996) suggested that the low volume transport of 2.2 Sv in transect 5 may have occurred because of the difficulties in computing geostrophic velocities from CTD transects.

The position of the SF presented here agrees with Jillett (1969) and Heath (1972) who observed the STW and SAW in the vicinity of the continental slope, and with Heath (1981a) who suggested that the SF may be influenced by the bathymetry of the continental slope. Chiswell's (1994b) EOF analysis, using a 2-year AVHRR SST data set also showed similar results, although this present study is more detailed.

The inshore position of the SF during the summer was consistent with Shaw and Vennell (2000a), who used

Table 3. Characteristics of the Southland Front [Mean \pm 95% Confidence Interval and (*s.d.*)], Defined by the Front-Following Algorithm (Shaw and Vennell, 2000b)^a

<i>a. The 3-Year (April 1989–March 1992) and Annual Time Scales</i>					
		1989 (Apr–Mar)	1990 (Apr–Mar)	1991 (Apr–Mar)	3-Year Total
Max no. images		94	109	74	277
Width, 2 <i>a</i> (km)		7.83 \pm 0.03 (4.42)	8.28 \pm 0.02 (4.77)	9.23 \pm 0.04 (5.20)	8.36 \pm 0.02 (4.8)
Temp. diff., 2 <i>b</i> (°C)		2.00 \pm <0.01 (0.73)	1.70 \pm <0.01 (0.61)	1.53 \pm <0.01 (0.59)	1.76 \pm <0.01 (0.68)
Temp. grad. (°C/km)		−0.33 \pm <0.01 (0.24)	−0.27 \pm <0.01 (0.20)	−0.23 \pm <0.01 (0.33)	−0.28 \pm <0.01 (0.25)
Temp., <i>T</i> ₀ (°C)		11.60 \pm 0.03 (2.29)	10.79 \pm 0.02 (1.81)	10.52 \pm 0.03 (2.04)	11.01 \pm 0.01 (2.29)
<i>b. The Seasonal Time Scales of 1989, 1990, and 1991</i>					
		Autumn ^b (Mar–May)	Winter (Jun–Aug)	Spring (Sep–Nov)	Summer (Dec–Feb)
1989	Max no. images	12	24	23	23
	Width, 2 <i>a</i> (km)	7.30 \pm 0.06 (4.04)	6.66 \pm 0.04 (3.9)	7.35 \pm 0.05 (4.2)	9.35 \pm 0.06 (4.75)
	Temp. diff., 2 <i>b</i> (°C)	1.62 \pm 0.01 (0.50)	2.33 \pm 0.01 (0.75)	1.77 \pm 0.01 (0.68)	2.03 \pm 0.01 (0.74)
	Temp. grad. (°C/km)	−0.28 \pm <0.01 (0.16)	−0.46 \pm 0.01 (0.33)	−0.32 \pm 0.01 (0.23)	−0.26 \pm <0.01 (0.15)
	Temp., <i>T</i> ₀ (°C)	11.54 \pm 0.03 (0.8)	9.18 \pm 0.02 (0.69)	10.83 \pm 0.04 (1.64)	14.34 \pm 0.04 (1.63)
1990	Max no. images	33	24	32	24
	Width, 2 <i>a</i> (km)	8.00 \pm 0.04 (4.43)	7.71 \pm 0.05 (4.76)	8.87 \pm 0.05 (4.83)	9.04 \pm 0.07 (4.86)
	Temp. diff., 2 <i>b</i> (°C)	1.94 \pm 0.01 (0.63)	1.76 \pm 0.01 (0.62)	1.56 \pm 0.01 (0.58)	1.72 \pm 0.01 (0.66)
	Temp. grad. (°C/km)	−0.30 \pm <0.01 (0.17)	−0.31 \pm <0.01 (0.24)	−0.23 \pm <0.01 (0.17)	−0.24 \pm <0.01 (0.16)
	Temp., <i>T</i> ₀ (°C)	12.39 \pm 0.03 (1.39)	9.33 \pm 0.01 (0.75)	9.97 \pm 0.02 (0.90)	13.56 \pm 0.03 (1.02)
1991	Max no. images	24	19	16	18
	Width, 2 <i>a</i> (km)	9.07 \pm 0.06 (5.34)	8.58 \pm 0.06 (5.35)	10.12 \pm 0.07 (5.05)	9.64 \pm 0.07 (4.66)
	Temp. diff., 2 <i>b</i> (°C)	1.52 \pm 0.01 (0.61)	1.49 \pm 0.01 (0.54)	1.60 \pm 0.01 (0.63)	1.70 \pm 0.01 (0.64)
	Temp. grad. (°C/km)	−0.24 \pm 0.01 (0.51)	−0.25 \pm 0.01 (0.22)	−0.19 \pm <0.01 (0.10)	−0.21 \pm <0.01 (0.12)
	Temp., <i>T</i> ₀ (°C)	12.55 \pm 0.02 (1.04)	8.88 \pm 0.02 (0.79)	9.01 \pm 0.03 (1.00)	13.10 \pm 0.03 (0.93)
<i>c. The Averaged Seasons for the 3 Years</i>					
Averaged Seasons		Autumn (Mar–May)	Winter (Jun–Aug)	Spring (Sep–Nov)	Summer (Dec–Feb)
Max no. images		74	67	71	65
Width, 2 <i>a</i> (km)		8.19 \pm 0.03 (4.73)	7.63 \pm 0.03 (4.74)	8.69 \pm 0.03 (4.81)	9.37 \pm 0.04 (4.77)
Temp. diff., 2 <i>b</i> (°C)		1.73 \pm <0.01 (0.63)	1.86 \pm <0.01 (0.72)	1.63 \pm <0.01 (0.63)	1.83 \pm 0.01 (0.70)
Temp. grad. (°C/km)		−0.28 \pm <0.01 (0.32)	−0.34 \pm <0.01 (0.28)	−0.25 \pm <0.01 (0.19)	−0.24 \pm <0.01 (0.15)
Temp., <i>T</i> ₀ (°C)		12.27 \pm 0.02 (1.24)	9.17 \pm 0.01 (0.76)	10.02 \pm 0.02 (1.35)	13.37 \pm 0.02 (1.36)

^a The less than sign represents a confidence interval less than 0.005.

^b No data for March 1989.

a different technique from AVHRR SST imagery to show that a SAW wisp (which is associated with the SF) extends north through the Mernoo Saddle and lies closer inshore during summer. Jillett (1969) also showed that the SF was further inshore during summer off Dunedin, however unlike Jillett's study, Table 1 indicated that the front was further offshore during spring. He showed that this inshore position was only a surface feature where the SAW had become less dense and moved over the STW.

Comparison of the Front-Following Algorithm with CTD data

For April 1993, the average position (\pm *s.d.*) of the SF recorded by the algorithm and meaned using the spatial bins was compared with the CTD data (upper 20 m) gathered in that month (Fig. 8). The characteristics used to define the water masses off the east coast of the South Island (Table 4) were based on Jillett (1969), Heath

(1972; 1981b), and Smith (1994). The mixing of water masses close to the 500 m isobath seen in the CTD data involved the STW and SAW, and was considered to be the region of the SF. The mixing of the water masses was defined from the TS plots from the April 1993 cruise (Shaw, 1998, Fig. A.1). The SAW wisp through the Mernoo Saddle is clearly visible from the CTD data (Fig. 8). Thus, the western side of the SAW extension (associated with the SF) through the Mernoo Saddle was followed using the algorithm and the results are presented for this month only. To find the average position of the SF through the Mernoo Saddle another path was created for the 220 km \times 20 km spatial bins to pass through the Saddle. The starting position of this second path was south of the Mernoo Saddle at a point corresponding to 500 km along the original northeast line, that is, at 2588.6 E km 5663.6 N km, NZMG (latitude 44°26'32"S, longitude 173°58'58"E). The direction of this 100 km path was north.

Table 4. Temperature and Salinity Characteristics of Water Masses off the East Coast of the South Island, New Zealand, Based on Jillett (1969), Heath (1972; 1981b), and Smith (1994)

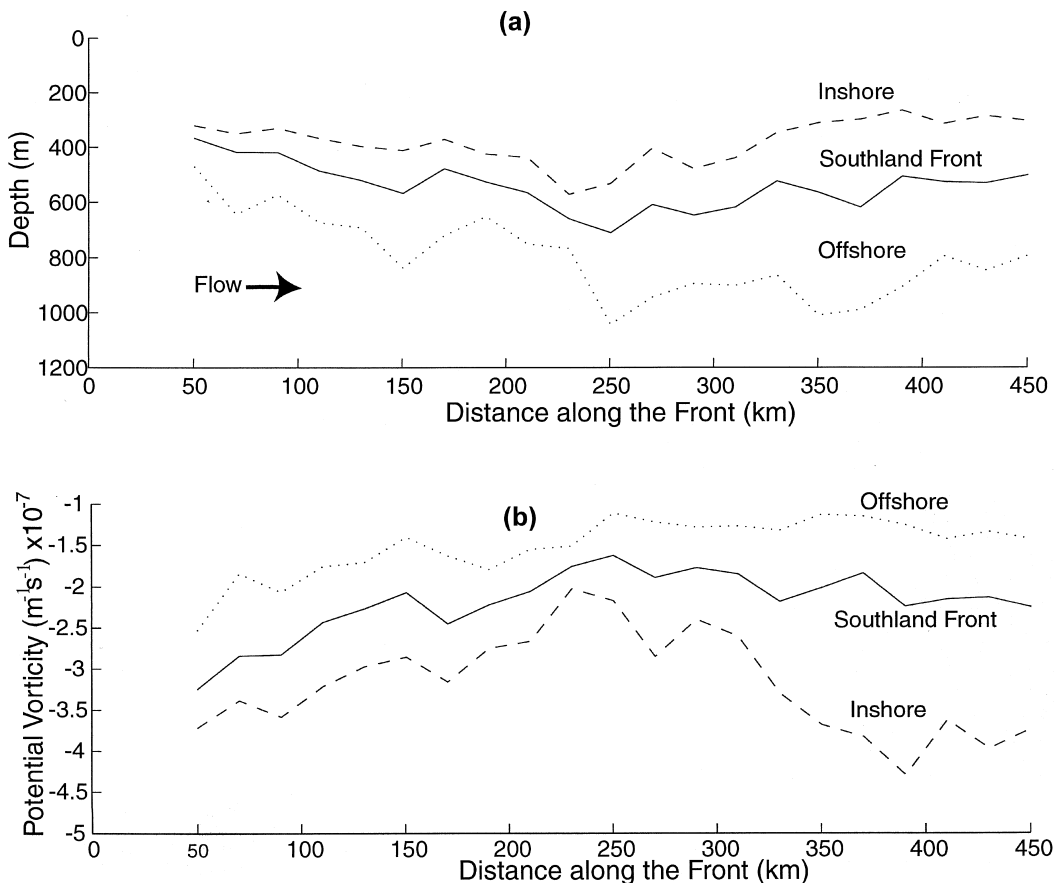
Water Mass	Temperature ($^{\circ}\text{C}$)	Salinity (psu)
Neritic water (NW)	9–14	33.8–34.6
Subtropical surface water (STW)	9–13	34.6–34.9
Subantarctic surface water (SAW)	7–12	34.3–34.5
Antarctic intermediate water (AIW)	4–6	34.3–34.4 @ depth 700–1200 m
Pacific deep water (PDW)	1–2	34.6–34.8 @ depth core about 3500 m

Figure 8 shows that the position of the SF (which also includes the western edge of the SAW wisp) defined by the algorithm is similar to that of the CTD data. The average position is within the mixing zone defined by the CTD observations. This supports the use of AVHRR SST data and the Front-Following Algorithm for detecting the position of the SF, even though only the skin temperature of the ocean is detected by the satellite. The western side of the SAW wisp (associated with the SF) was inshore from the 500 m isobath. This was expected as the Front was further inshore in summer and autumn (Table 1), and the Wisp meandered inshore from the 500

m isobath, especially during summer (Shaw and Vennell, 2000a). There are two gaps in the average position of the SF in Figure 8. The first gap (offshore from Oamaru) is due to the lack of AVHRR SST data. The second gap occurs off Banks Peninsula, where the northeast binning path finishes and the northern averaging path through the Mernoo Saddle begins.

An example of the subsurface structure of potential temperature and salinity of the water masses can be seen in Figure 9 to 300 dbars from the CTD transect 5. Both plots reveal that the waters offshore from the 500 m isobath were more stratified compared with the waters in-

Figure 7. The mean position of the Southland Front from the three year AVHRR SST data with respect to depth (a), from which potential vorticity (f/D) was estimated along the Front (b). The dotted and dashed lines represent the depth and potential vorticity at 1 *s.d.* from the mean position (offshore and inshore, respectively).



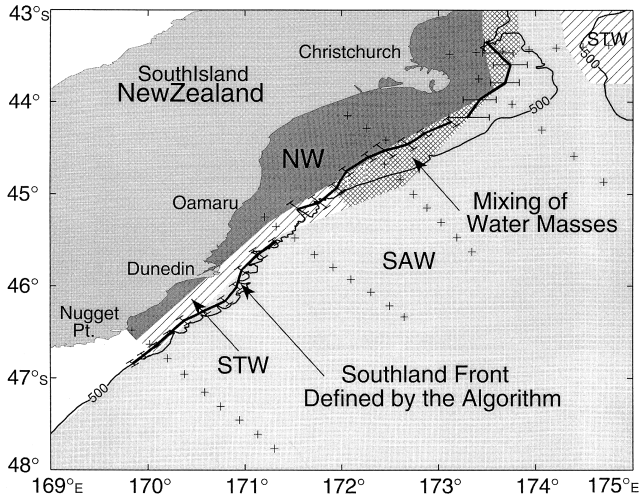


Figure 8. The mean position (± 1 s.d.) of the Southland Front in April 1993 as recorded by the algorithm overlaid onto the surface water masses identified from the conductivity temperature depth (CTD) data from the NIWA (NZOI) cruise 3006 in April 1993. The 500 m isobath represents the midpoint of the continental slope. The crosses indicate the positions of the CTD stations. NW: Neritic Water mass; STW: Subtropical Surface Water mass; SAW: Subantarctic Surface Water mass.

shore, and that a relatively sharp temperature and salinity gradient occurs within the vicinity of the 500 m isobath. The algorithm was used to determine the position of the SF from a cloud-free AVHRR SST image 2 days later. The surface position calculated from the algorithm is shown in Figure 9a, within the position of the SF defined by Table 4 (shown in Fig. 9b). Transect 5 shows the position of the subsurface structure of the SF being represented at the surface.

Characteristics of the Southland Front

If the structure of the SF was constant along its length, then it would be expected that the S.D. would be small given the amount of data. The observed high s.d.'s suggest that the SF has a significant variation along its length. This high variability was expected as there was a large variation in gradient of the continental slope shown in Figure 1b.

The mean width across the SF determined in this study as 8.36 km from the 3-year AVHRR SST data, was very narrow compared with Heath (1975, Figs. 8–13), who described the SF as a region of gradual change in hydrological properties. However, Heath could not resolve a narrow width across the SF as his hydrocast stations (bottle casts) were 20–60 km apart. Holliday and Read (1998) calculated the average latitudinal width of the South STF from ship data south of South Africa as 107 km, Lutjeharms and Valentine (1984) calculated the average latitudinal width of the combined (North and

South) STF in this region as 225.1 km with a s.d. of 140.6 km.

The mean temperature (T_0) at the interface of the SF decreased significantly between April 1989 to March 1992. This agrees well with a 10-year fitted AVHRR SST time series in the same region showing similar effects due to the El Niño event (Shaw et al., 1999). Shaw et al. (1999) found that the STW and SAW were in phase and both water masses had similar interannual trends, calculated from the 10-year data set.

There is a direct relationship between SST gradients and the velocity induced by large scale oceanic fronts. The decrease in SST gradient over the three years (Table 3a) was highly significant, and may indicate a decrease in induced velocity in this part of the global STF. Although this study covers a relatively short time frame, it was intriguing that this decrease in SST gradient coincided with the decrease in Southern Oscillation Index (SOI). This suggests that the northward flow along the SF may have decreased with the El Niño. Meyers (1996) found that the Indonesian throughflow current system (which flows from the Pacific Ocean to the Indian Ocean) decreased during the El Niño years of 1986–1987 and 1991–1994. However, more spatial and temporal data, including data from the Tropical South Pacific region would be required to determine if a decrease in velocity of the SF occurred as a consequence of El Niño and what effects this may have.

The temperature gradient was consistently higher in winter than the other seasons during the three years, suggesting a greater induced velocity in this season. The temperature gradient is a function of a and b , and, as the temperature difference showed little seasonality, this suggests that the temperature gradient across the front may be influenced by its width. Chiswell (1994b) also found that the strongest SST gradient of the front occurred in late winter, although direct comparisons are difficult due to the coarse sampling resolution in his study. The magnitude of the average gradient of the SF over the three years ($0.28^\circ\text{C}/\text{km}$) is greater than the $0.047^\circ\text{C}/\text{km}$ (\pm s.d. of $0.043^\circ\text{C}/\text{km}$) measured across the combined (South and North) STF south of South Africa from ship data (Lutjeharms and Valentine, 1984).

Figure 6b indicated that spatially, the mean temperature difference decreased along the SF beyond Dunedin, which implied that the STW and SAW had different thermal properties. These water masses were examined further by comparison with a fitted 10-year time-series of AVHRR SST data (Shaw et al., 1999). The fitted temperature time-series consisted of a single sinusoid and an interannual trend component for 10 selected sites extracted from STW, SAW, and the Neritic Water mass (NW). Four sites (STW and SAW) straddled the SF, two off Oamaru at latitude 45°S , and another two sites off Dunedin at latitude 46°S . Differences in temperature between latitudes 45°S and 46°S were calculated for SAW

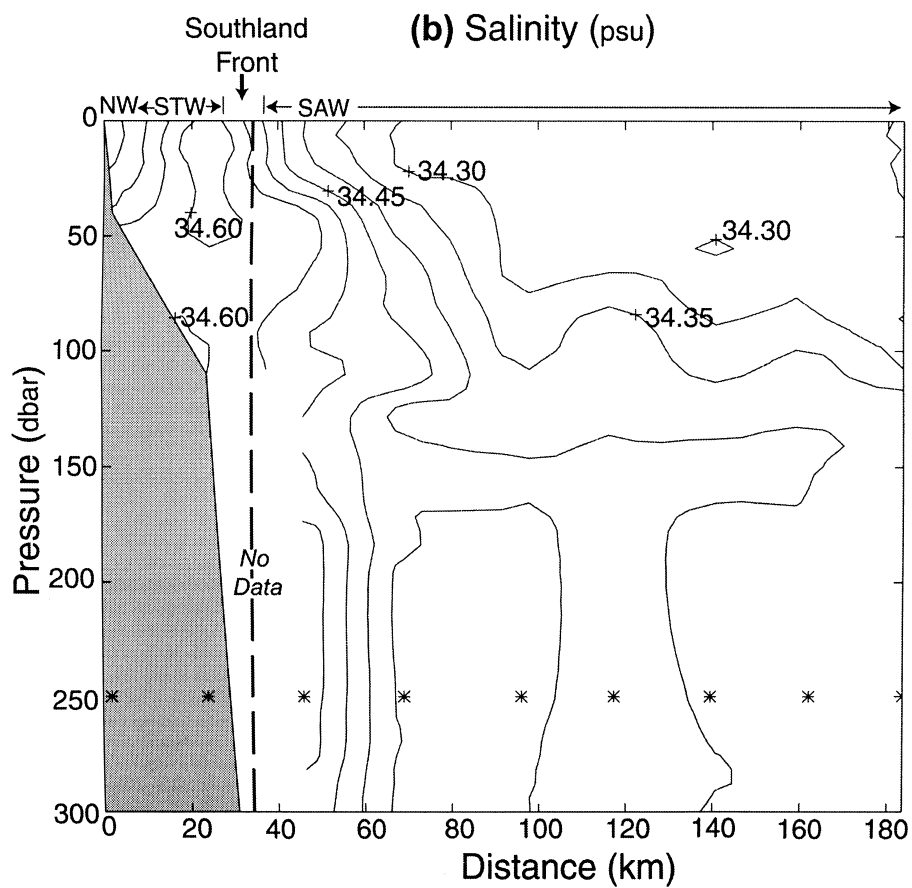
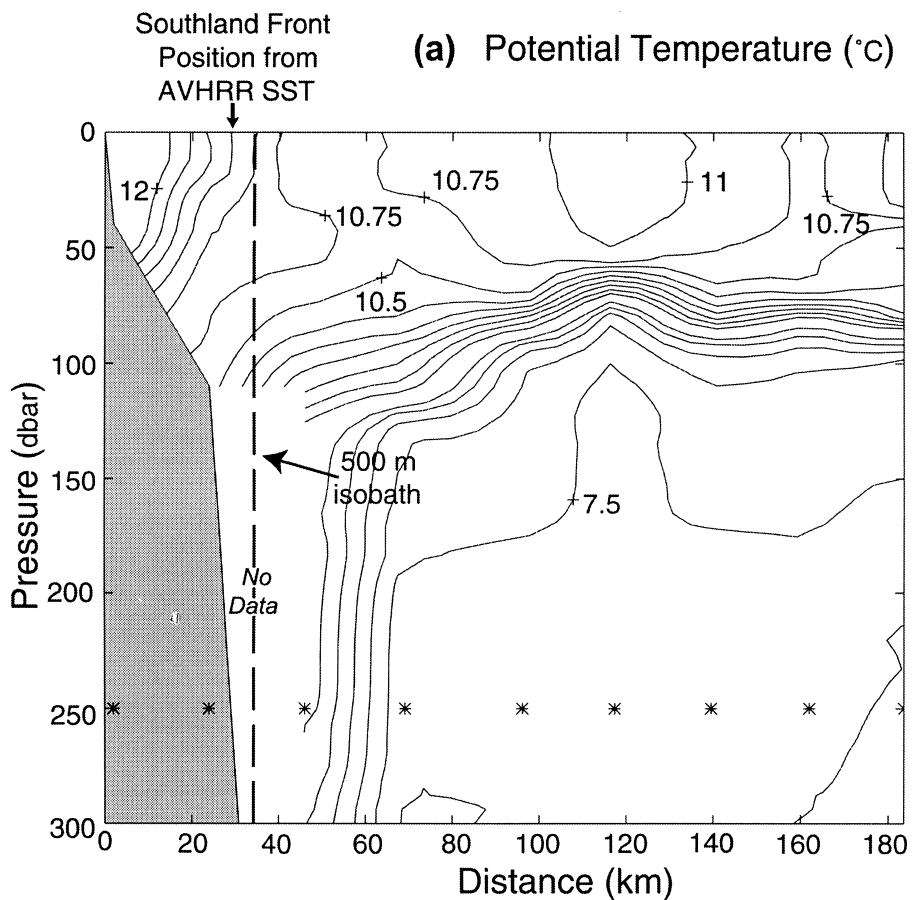


Figure 9. The conductivity temperature depth (CTD) profile of transect 5 showing potential temperature (a) and salinity (b) in the vicinity of the Southland Front (SF). The position of the SF defined by the Front-Following Algorithm (Shaw and Vennell, 2000b) from an AVHRR SST image 2 days later is shown in a). The position of the SF defined by Table 4 is shown in b). CTD data from the NIWA (NZOI) cruise 3006, April 1993.

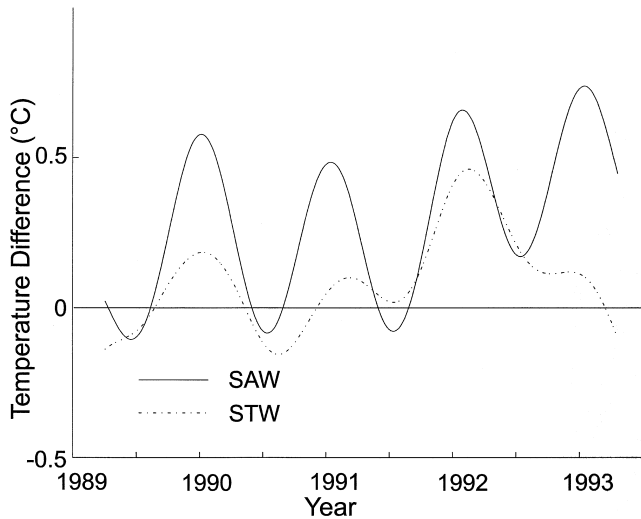


Figure 10. Differences in temperature between latitudes 45°S and 46°S for SAW and STW from a fitted temperature time series (Shaw et al., 1999). A positive difference indicates that the water masses (SAW or STW) at latitude 45°S were warmer than at 46°S.

and STW and are shown in Figure 10. The relative seasonality within both the STW and the SAW between the latitudes shows that there was a maximum rate of warming in summer and cooling during winter. During the southern hemisphere spring, summer, and autumn, the SAW appears to warm more than the STW as they both travel northwards along the continental slope. Assuming that the amount of solar heating acting on both water masses is similar, then it seems that the SAW may be more sensitive to the effect of surface heating than the STW. Figure 9 indicates that there was more stratification within the water column of the SAW which may result in greater temperature increases within the mixed water column compared with the STW. In the winter, the magnitudes of the relative temperatures within the SAW and STW were much smaller, similar, and mostly negative as both water masses flowed northwards. Thus, both water masses at latitude 45°S were generally cooler than at latitude 46°S during winter. This cooling as the flow moves north may be a result of a greater net heat loss to the atmosphere in the winter. However, both water masses had positive relative values during the winter of 1992 (i.e., warming from 46°S to 45°S). The reason for this is not clear. Another potential factor contributing to the decrease in the temperature difference (2b) shown in Figure 6b may be cross-frontal mixing induced by the plumes within the Canterbury Bight. Cloud formation has been known to occur on the SAW side of the STF off the east coast of New Zealand (Heath, 1973). However, the effect of this on the temperature difference between the two water masses is not known.

CONCLUSION

The mean position of the SF (part of the Subtropical Front) determined from a 3-year AVHRR SST data set was constrained by the local bathymetry to approximately the 500 m isobath. This may be related to topographic steering. Seasonally, the position of the SF was found to be inshore during summer. The characteristics that describe the profile at the interface of the SF were calculated from the 3-year AVHRR SST data set as: a mean width of 8.36 km across the Front; a mean temperature difference between the STW and SAW of 1.76°C; a mean temperature at the interface of 11.01°C; and a SST gradient of $-0.28^{\circ}\text{C}/\text{km}$ across the SF. The SST difference decreased northeastwards along the SF, indicating that the two water masses had different thermal properties, possibly due to different stratification. The SST gradient was found to be strongest in the winter and the width was narrowest in this season, suggesting that there is an increase in induced velocity along the SF in winter. The SST gradient decreased from April 1989 to March 1992, coinciding with a decrease in the SOI. The Front-Following Algorithm provided a good technique to describe the position and characteristics of the SF using AVHRR SST imagery over the time scales examined.

The authors wish to thank John Simpson from the School of Ocean Science, University of Wales Bangor, United Kingdom for his useful comments. Thanks to Chris Old and Mark Gibbs of the Department of Marine Science, University of Otago, New Zealand for their suggestions. Thanks to Ted Barnes, formerly of Landcare Research New Zealand Ltd for the AVHRR SST images; to NIWA (NZOI) for allowing the first author to participate in the cruise 3006 in April 1993, on the ship RV Akademik Lavrentyev; and to the cruise leader Steve Chiswell, for access to the CTD data. Special thanks to Peter Challenor, Adrian New, and John Hemmings of the James Rennell Division, Southampton Oceanography Centre, United Kingdom for their valuable input. Many thanks to the anonymous referees for their very helpful comments. This study was funded by Research Grants provided by the University of Otago, New Zealand.

REFERENCES

- Barnes, E. J. (1985), Eastern Cook Strait region circulation inferred from satellite-derived, sea-surface temperature data. *N.Z. J. Mar. Freshwat. Res.* 19:405–411.
- Barton, I. J. (1982), Accurate SST measurements from AVHRR data. In *Applications of Environmental Satellites*, CSIRO, Division of Groundwater Research, Division of Fisheries Research/Western Australia Institute of Technology, Perth, pp. 5.12.1–5.12.9.
- Belkin, I. M., and Gordon, A. L. (1996), Southern Ocean from the Greenwich Meridian to Tasmania. *J. Geophys. Res. Oceans* 101(C2):3675–3696.
- Bradford-Grieve, J. M., Lewis, K. B., and Stanton, B. R. (1991), Advances in New Zealand oceanography, 1967–91. *N.Z. J. Mar. Freshwat. Res.* 25:429–441.

- Burling, R. W. (1961), Hydrology of circumpolar waters south of New Zealand, Bulletin 143, N.Z. Department of Scientific and Industrial Research, Wellington, 66 pp.
- Chiswell, S. M. (1994a), Acoustic Doppler current profile measurements over the Chatham Rise. *N. Z. J. Mar. Freshwat. Res.* 28:167–178.
- Chiswell, S. M. (1994b), Variability in sea surface temperature around New Zealand from AVHRR images. *N. Z. J. Mar. Freshwat. Res.* 28:179–192.
- Chiswell, S. M. (1996), Variability of the Southland Current. *N. Z. J. Mar. Freshwat. Res.* 30:1–17.
- Deacon, G. E. R. (1937), The hydrology of the South Ocean. *Discovery Rep.* 15:1–124.
- Deacon, G. E. R. (1945), Water circulation and surface boundaries in the oceans. *Quart. J. Roy. Meteorol. Soc.* 71:11–25.
- Garner, D. M. (1954), Sea surface temperature in the south-west Pacific Ocean, from 1949–1952. *N. Z. J. Sci. Technol.*: 285–303.
- Garner, D. M. (1959), The subtropical convergence in New Zealand surface waters. *N. Z. J. Geol. Geophys.* 2:315–337.
- Heath, R. A. (1972), The Southland Current. *N. Z. J. Mar. Freshwat. Res.* 6(3):497–533.
- Heath, R. A. (1973), Low cloud boundaries coincident with oceanic convergences. *N. Z. J. Mar. Freshwat. Res.* 7(3): 209–216.
- Heath, R. A. (1975), Oceanic circulation and hydrology off the southern half of the South Island, New Zealand, Memoir No. 72, New Zealand Oceanographic Institute, Wellington, 36 pp.
- Heath, R. A. (1981a), Oceanic fronts around southern New Zealand. *Deep-Sea Res.* 28(6):547–560.
- Heath, R. A. (1981b), *Physical Oceanography of the Waters over the Chatham Rise*, (DSIR) Special Edition (Summary No. 18), New Zealand Oceanographic Institute, Wellington.
- Heath, R. A. (1983), Observations on the Chatham Rise currents. *N. Z. J. Mar. Freshwat. Res.* 17(3):321–330.
- Holliday, N. P., and Read, J. F. (1998), Surface oceanic fronts between Africa and Antarctica. *Deep-Sea Res.* 45 (2–3): 217–238.
- Jackson, G. D., Shaw, A. G. P., and Lalas, C. (2000), Distribution and biomass of two squid species off southern New Zealand: *Nototodarus sloanii* and *Moroteuthis ingens*. *Polar Biol.* 23(10):699–705.
- Jillett, J. B. (1969), Seasonal hydrology of waters off the Otago Peninsula, South-Eastern New Zealand. *N. Z. J. Mar. Freshwat. Res.* 3(3):349–375.
- Lands and Survey (1973), New Zealand Map Grid, Technical Circular 1973/32 Distribution E1, Land Information New Zealand, P.O. Box 5501, Wellington, New Zealand.
- Lutjeharms, J. R. E., and Valentine, H. R. (1984), Southern ocean thermal fronts south of Africa. *Deep-Sea Res.* 31(12): 1461–1475.
- Lutjeharms, J. R. E., Valentine, H. R., and van Ballegooyen, R. C. (1993), On the subtropical convergence in the south Atlantic Ocean. *S. Afr. J. Sci.* 89:552–559.
- Marshall, D. (1995a), Influence of topography on the large-scale ocean circulation. *J. Phys. Oceanogr.* 25(7):1622–1635.
- Marshall, D. (1995b), Topographic steering of the Antarctic Circumpolar Current. *J. Phys. Oceanogr.* 25(7):1636–1650.
- Meyers, G. (1996), Variation of Indonesian throughflow and the El Niño—Southern Oscillation. *J. Geophys. Res. Oceans* 101(C5):12,255–12,263.
- Özgökmen, T. M., Chassignet E. P., and Paiva, A. .M. (1997), Impact of wind forcing, bottom topography, and inertia on midlatitude jet separation in a quasigeostrophic model. *J. Phys. Oceanogr.* 27(11):2460–2476.
- Pickard, G. L. (1975), *Descriptive Physical Oceanography—An Introduction*, Pergamon, Oxford.
- Pond, S., and Pickard, G. L. (1983), *Introduction, Dynamical Oceanography*, Pergamon, New York.
- Reid, J. L., and Mantyla, A. W. (1976), The effect of the geostrophic flow upon coast sea level elevations in the Northland North Pacific Ocean. *J. Geophys. Res.* 81(18):3100–3110.
- Rintoul S. R., Donguy J. R., and Roemmich, D. H. (1997), Seasonal evolution of upper ocean thermal between Tasmania and Antarctica. *Deep-Sea Res.* 44(7):1185–1202.
- Shaw, A. G. P. (1998), The temporal and spatial variability of the Southland Front, New Zealand using AVHRR SST imagery, Ph.D. thesis, University of Otago, Dunedin, New Zealand, 248 pp.
- Shaw, A. G. P., Kavalieris, L., and Vennell, R. (1999), Seasonal and inter-annual variability of SST off the east coast of the South Island, New Zealand. *Geocarto Int.* 14(3):27–32.
- Shaw, A. G. P., and Vennell, R. (2000a), Variability of water masses through the Mernoo Saddle, South Island, New Zealand. *N. Z. J. Mar. Freshwat. Res.* 34(1):103–116.
- Shaw, A. G. P., and Vennell, R. (2000b), A front-following algorithm for AVHRR SST imagery. *Remote Sens. Environ.* 72 (3):317–327.
- Smith, A. M. (1994), *Background Report 4: Eastward to the Sea: A Scientific Review of the Otago's Coastal Marine Area*, Otago Regional Council, Dunedin, New Zealand.
- von Storch, H., and Zwiers, F. W. (1999), *Statistical Analysis in Climate Research*, Cambridge University Press, Cambridge.